# Selective enrichment of high-affinity clade II N2O-reducers in a mixed culture

Laureni, Michele; Corbera-Rubio, Francesc; Kim, DaeHyun Daniel; Browne, Savanna; Roothans, Nina; Weissbrodt, David G; Olavarria, Karel; de Jonge, Nadieh; Yoon, Sukhwan; Pabst, Martin

**DOI**
10.1093/ismeco/ycaf022

**Publication date**
2025

**Document Version**
Final published version

**Published in**
ISME Communications

**Citation (APA)**
Laureni, M., Corbera-Rubio, F., Kim, D. D., Browne, S., Roothans, N., Weissbrodt, D. G., Olavarria, K., de Jonge, N., Yoon, S., Pabst, M., & van Loosdrecht, M. C. M. (2025). Selective enrichment of high-affinity clade II N2O-reducers in a mixed culture. *ISME Communications*, *5*(1), Article ycaf022. https://doi.org/10.1093/ismeco/ycaf022

ISME Communications, 2025, 5(1), ycaf022
https://doi.org/10.1093/ismeco/ycaf022
Advance access publication: 5 February 2025
Original Article

# Selective enrichment of high-affinity clade II $N_2O$-reducers in a mixed culture

Michele Laureni[1,*], Francesc Corbera-Rubio[1], DaeHyun Daniel Kim[2,5], Savanna Browne[1], Nina Roothans[1], David G. Weissbrodt[3], Karel Olavaria[1], Nadieh de Jonge[4], Sukhwan Yoon[2], Martin Pabst[1], Mark C.M. van Loosdrecht[1]

[1]Department of Biotechnology, Delft University of Technology, Van der Maasweg 9, Delft, HZ NL- 2629, The Netherlands
[2]Department of Civil and Environmental Engineering, Korea Advanced Institute of Science and Technology, Daehakro 291, KAIST, Daejeon 34141, South Korea
[3]Department of Biotechnology and Food Science, Norwegian University of Science and Technology, Sem Sælands vei 8, Trondheim 7034, Norway
[4]Department of Chemistry and Bioscience, Aalborg University, Fredrik Bajers Vej 7H, Aalborg DK-9220, Denmark
[5]Present address: Department of Civil and Environmental Engineering, University of California, Berkeley, CA, USA

*Corresponding author. Present address: Department of Water Management, Delft University of Technology, Stevinweg 1, 2628 CN Delft, the Netherlands. E-mail: m.laureni@tudelft.nl

## Abstract

Microorganisms encoding for the $N_2O$ reductase (NosZ) are the only known biological sink of the potent greenhouse gas $N_2O$ and are central to global $N_2O$ mitigation efforts. Clade II NosZ populations are of particular biotechnological interest as they usually feature high $N_2O$ affinities and often lack other denitrification genes. We focus on the yet-unresolved ecological constraints selecting for different $N_2O$-reducers strains and controlling the assembly of $N_2O$-respiring communities. Two planktonic $N_2O$-respiring mixed cultures were enriched at low dilution rates under limiting and excess dissolved $N_2O$ availability to assess the impact of substrate affinity and $N_2O$ cytotoxicity, respectively. Genome-resolved metaproteomics was used to infer the metabolism of the enriched populations. Under $N_2O$ limitation, clade II $N_2O$-reducers fully outcompeted clade I affiliates, a scenario previously only theorized based on pure-cultures. All enriched $N_2O$-reducers encoded and expressed the sole clade II NosZ, while also possessing other denitrification genes. Two *Azonexus* and *Thauera* genera affiliates dominated the culture, and we hypothesize their coexistence to be explained by the genome-inferred metabolic exchange of cobalamin intermediates. Under excess $N_2O$, clade I and II populations coexisted; yet, proteomic evidence suggests that clade II affiliates respired most of the $N_2O$, *de facto* outcompeting clade I affiliates. The single dominant $N_2O$-reducer (genus *Azonexus*) notably expressed most cobalamin biosynthesis marker genes, likely to contrast the continuous cobalamin inactivation by dissolved cytotoxic $N_2O$ concentrations (400 $\mu$M). Ultimately, our results strongly suggest the solids dilution rate to play a pivotal role in controlling the selection among NosZ clades, albeit the conditions selecting for genomes possessing the sole *nosZ* remain elusive. We furthermore highlight the potential significance of $N_2O$-cobalamin interactions in shaping the composition of $N_2O$-respiring microbiomes.

**Keywords:** nitrous oxide, $N_2O$ respiration, clade II NosZ, cobalamin, vitamin b12, $N_2O$ cytotoxicity, mixed culture, non-axenic enrichment

## Introduction

Nitrous oxide ($N_2O$) is a potent greenhouse gas, with a global warming potential almost 300 times higher than $CO_2$, and it is the predominant ozone-depleting substance in the atmosphere [1]. $N_2O$ emissions have been increasing globally at a rate of 17 Tg N $y^{-1}$ over the last decade [2], and this rise is expected to continue if no mitigation efforts are put in place [1]. Most of the produced $N_2O$ results from microbially mediated reactions in managed and engineered ecosystems characterized by high nitrogen loads, such as agricultural soils and wastewater treatment plants (WWTPs) [3, 4]. In-depth understanding of the microbiology underlying $N_2O$ production and consumption is paramount in emission mitigation endeavors.

$N_2O$ is produced primarily as a by-product of the first nitrification step, namely the biological oxidation of ammonia ($NH_3$) to nitrite ($NO_2^-$), or during incomplete denitrification [5, 6]. Denitrification is the sequential reduction of dissolved nitrate ($NO_3^-$) and $NO_2^-$ to dinitrogen gas ($N_2$), with nitric oxide (NO) and $N_2O$ as obligate free intermediates [7]. Each reduction step is catalyzed by distinct enzymes and can function as an independent energy-conserving reaction [4, 7, 8]. Denitrification can be performed by a single microorganism (termed "generalist") or a consortium of cooperating "specialists", each of them performing one or few nitrogen oxides reductions [9]. As such, denitrification can act as a source or a sink of $N_2O$ depending on the genetic and metabolic repertoire of the microbial community members, and the environmental conditions [10, 11]. Importantly, the reduction of $N_2O$ to $N_2$ catalyzed by the $N_2O$-reductase (NosZ), the last step of the denitrification pathway, is the only known biological $N_2O$ sink [4].

The ability to reduce $N_2O$ is taxonomically widely distributed among diverse microbial groups [12], and the *nosZ* gene evolved

**Received:** 20 February 2024. **Revised:** 28 June 2024. **Accepted:** 4 February 2025

in two phylogenetically distinct lineages, namely clade I and II [4]. Interestingly, clade II NosZ appears to be more often encoded in genomes of non-denitrifying (specialist) $N_2O$-reducers, namely microorganisms lacking other denitrifying enzymes that represent possible net $N_2O$ sinks [4, 13, 14]. Limited pure culture-based observations suggests that clade II organisms feature higher affinities for $N_2O$ than clade I populations, albeit at usually lower maximum specific growth rates [15, 16]. On these grounds, clade II $N_2O$-reducers hold the potential to further curb emissions by reducing residual dissolved $N_2O$ concentrations, irrespective of their denitrifying capacity.

Denitrifying communities dominated by $N_2O$-reducing specialists [17] and rich in clade II affiliates are ubiquitous [9, 12, 18–23]. The abundance of clade II populations has been reported to inversely correlate with $N_2O$ emissions from soils [10, 24, 25]. High relative abundances of clade II $N_2O$-reducers have been obtained in lab-grown biofilms [15, 26, 27]. In their seminal chemostat work, Conthe and co-workers [28, 29] reported a marked increase in clade II *nosZ* gene abundance when the dilution rate was decreased from 0.086 to 0.027 $h^{-1}$. Yet, to date, no enrichment has resulted in the selection of sole clade II organisms. Different traits such as the preferred electron donor [30], the sensitivity to other electron acceptors like $NO_3^-$ [31] and $O_2$ [30], or the required presence of other nitrogen oxides [32] may also contribute to clades selection. $N_2O$ itself may result in direct cytotoxicity, hindering microbial growth by selectively inactivating vitamin $B_{12}$ [33], with implications on community assembly that remain largely unknown. Resolving the ecological constraints controlling the selection of different $N_2O$-reducers would greatly benefit both biotechnological designs and our understanding of the biosphere response to a rapidly changing climate.

We postulate that the high solids dilution rates used in previous studies prevented the selection of clade II $N_2O$-reducers [28, 29]. To verify our hypothesis, two $N_2O$-respiring mixed cultures were enriched under limitation of either electron donor (acetate) and electron acceptor ($N_2O$), and an ultrafiltration membrane was used to impose a solids dilution rate five times lower than ever tested. We employed continuous chemostat reactors to select, by design, for organisms with the highest affinity for the growth-limiting substrate [34], enabling direct comparisons without requiring the kinetic characterization of individual strains. The taxonomy and metabolic potential of the dominant community members at steady-state were identified via genome-resolved metagenomics. Shotgun metaproteomics was used to estimate the relative biomass contribution and infer the actual metabolism of each organism. Under $N_2O$-limiting conditions we successfully cultivated a mixed culture in which all $N_2O$-reducers encoded and expressed the sole clade II NosZ, while still the conditions were not selective enough for specialist $N_2O$-reducers. Additionally, metagenomic and metaproteomic data suggest a potential role of vitamin $B_{12}$ cross-feeding in the assembly of $N_2O$ converting communities, which has not been previously reported.

# Materials and methods

## Continuous enrichments

Two identical glass, continuous-flow membrane bioreactors (MBR) with a working volume of 2 L (Applikon, Delft, the Netherlands) were operated with acetate and $N_2O$ as sole electron donor and acceptor, respectively. To allow for direct comparisons, the set-up was identical to the one used by Conthe and co-workers [29]. The sole difference was the use in our set-up of a custom-made, submerged ultrafiltration membrane module [35] to uncouple the solids retention time (SRT) and the hydraulic retention time (HRT). In both MBRs, the HRT was maintained at 2.8 ± 0.3 d. The SRT was set at 6.9 ± 1.0 d, equivalent to a biomass dilution rate (D) of 0.006 ± 0.001 $h^{-1}$ (Table 1). The imposed D was lower than the growth rate reported for clade II *nosZ*-possessing *Anaeromyxobacter dehalogenans* 2CP-C (0.0076 $h^{-1}$), the slowest-growing $N_2O$-reducing bacterium examined by [16], and the minimum dilution rate (0.027 $h^{-1}$) that has been applied in previous non-axenic $N_2O$-reducing chemostat works [29]. The temperature was controlled at 20 ± 1°C, and the pH was maintained at 7.0 ± 0.1 with 1 M HCl and 1 M NaOH. Stirring at 750 rpm was ensured by two six-bladed flat turbines. Two independent 5850S mass-flow controllers (Brooks, Philadelphia, PA) were used in each MBR to mix pure $N_2O$ and $N_2$, and achieve the target overall gas flow and $N_2O$ concentration (Fig. 1). The carbon and nitrogen sources were provided separately. The two mineral media contained per liter: 90.5 mmol $CH_3COONa{\cdot}3H_2O$ or 26.4 mmol $NH_4Cl$ (anabolic nitrogen source), respectively, additionally to 7.4 mmol $KH_2PO_4$, 2.1 mmol $MgSO_4{\cdot}7H_2O$, 0.5 mmol NaOH, 2 mg yeast extract and 2.5 ml of trace element solution [36]. The first MBR operated under acetate limitation and $N_2O$ excess (hereafter referred to as *$N_2$Oexc*) was inoculated directly with activated sludge from the Harnaschpolder WWTP (Delft, the Netherlands). Excess $N_2O$ conditions, defined as no detectable acetate in the effluent, were achieved with influent acetate and $N_2O$ loads of 31.6 ± 2.0 and 382 ± 25 mmol/d, respectively, after a 30-days start-up phase. The second MBR operated under $N_2O$ limitation (*$N_2$Olim*) was inoculated with biomass collected from *$N_2$Oexc* after 98 days of operation. $N_2O$ limiting conditions in *$N_2$Olim* were reached on day 60, and maintained until day 95 at influent acetate and $N_2O$ loads of 46.1 ± 1.5 and 84 ± 2.1 mmol/d, respectively (Fig. 1). The residual acetate concentration in *$N_2$Olim* was 23.7 ± 5.5 mmol/L. Occasional growth on the MBR walls and membrane was cleaned on a weekly basis.

## Nitrite reduction batch tests

We aimed to quantify the long-term dynamics of the denitrification potential of the enrichments respiring exclusively $N_2O$. To this end, the maximum biomass-specific nitrite reduction rate ($q_{NO2^-}$; $mmol_{NO2^-}{\cdot}mmol_X^{-1}{\cdot}h^{-1}$) was used as denitrification proxy and quantified in batch. One liter of fresh reactor effluent was collected under anoxic conditions, via continuous $N_2$-sparging of the effluent collection vessel with $N_2$ gas, and centrifuged at 4200 rpm for 20 min at room temperature. The recovered pellet was re-suspended in $N_2$-sparged base mineral medium without ammonium or acetate, with the same composition as detailed above. Based on the biomass concentration measured in the chemostat, the cells were re-suspended to a concentration of 0.9 ± 0.2 $g_{VSS}{\cdot}L^{-1}$. Subsequently, 50 ml of cell suspension were aliquoted in 112 ml serum bottles. The bottles were sealed with rubber stoppers, and anoxic conditions were achieved by flushing with $N_2$ for 20 min. After overnight incubation, appropriate volumes of anoxic stock-solutions of $NH_4Cl$, $CH_3COONa{\cdot}3H_2O$, and $NaNO_2$ were added to reach the target initial concentrations of 2.1 mmol $NH_4^+{\cdot}L^{-1}$, 1.2 mmol $CH_3COO^-{\cdot}L^{-1}$, and 1.1 mmol $NO_2^-{\cdot}L^{-1}$. The frequency of bulk liquid sampling (4 mL) depended on biomass activity. Samples were immediately centrifuged for 5 min (4200 rpm, 4°C), and the supernatant was kept for further analysis. The volumetric $NO_2^-$ consumption rate was determined by calculating the slope of the linear regression of at least four nitrate concentration points measured during each batch. Average and standard deviations were obtained from replicate

bottles. Subsequently, the biomass-specific reduction rates were calculated by dividing the volumetric rates by the corresponding experimentally determined biomass concentration. The resulting standard deviations were calculated based on the average and standard deviations of the volumetric rates and biomass concentrations using linear error propagation. Initial and final acetate concentrations were measured to confirm non-limiting conditions. All tests were performed in an Incubator Hood TH30 (Edmund Bühler GmbH, Bodelshausen, Germany) at 20°C and 150 rpm. Negative controls with autoclaved biomass were also included. The pH remained in the range 7–8 without external control.

## Analytical procedures and calculations

Samples for influent and effluent supernatant analysis were centrifuged at 4°C and 13 000 rpm for 5 min, stored at −20°C, and analysed within less than 6 days. Bulk $NH_4^+$, $NO_2^-$ and $NO_3^-$ concentrations were measured spectrophotometrically with the Gallery™ Discrete Analyzer (Thermo Fisher Scientific). Acetate concentration was measured by high-performance liquid chromatography (Vanquish Core HPLC, Thermo Fisher Scientific) using an Aminex HPX-87H column (300 × 7.8 mm; Bio-Rad, Waters Chromatography B.V.), calibrated with standard solutions ranging from 0 to 250 mM. In- and off-gas $N_2O$ concentrations were continuously monitored online by a Rosemount NGA 2000 off-gas analyser (Emerson). Before reaching the analyser, the off-gas was dried in a condenser operated with water at 4°C using a cryostat bath (Lauda). $N_2O$ concentrations in the in- and off-gas of *$N_2$Oexc* exceeded the off-gas analyser range, thus weekly grab-samples were measured with a CP-3800 gas chromatograph (Varian). The concentrations of total and volatile suspended solids (TSS, VSS) in the mixed liquors were determined according to standard methods [37], and an average biomass composition of $CH_{1.8}O_{0.5}N_{0.2}$ [38] was assumed for downstream molar calculations. All stoichiometric yields (Table 1) were calculated as the ratio of the corresponding steady-state volumetric conversion rates (Table S1) after data reconciliation using the software Macrobal [39]. The resulting standard deviations were calculated based on the average and standard deviations of the individual volumetric rates using linear error propagation. The biomass-specific acetate consumption rate for maintenance was estimated by linear regression of the growth yields on acetate over the D range covered by this study and [29] (Fig. S1). Dissolved $N_2O$ concentrations were estimated from the average off-gas $N_2O$ concentrations with a Henry's constant of $2.4{\cdot}10^{-4}$ mmol/(L·Pa) [40].

## Metagenomics

*Metagenome sequencing.* Samples for metagenomic analysis were taken on days 123 (*$N_2$Oexc*) and 83 (*$N_2$Olim*). DNA was extracted using the DNeasy UltraClean Microbial Kit (Qiagen, The Netherlands). Library preparation and metagenomic sequencing were performed by Novogene Ltd. (Hongkong, China) on HiSeq platform (Illumina Inc., CA). Libraries were generated from 1 $\mu$g DNA per sample using the NEBNext Ultra DNA Library Prep Kit (NEB #E7645, USA) following the manufacturer's instructions. DNA was fragmented by sonication to a size of 350 bp, and DNA fragments were end-polished, A-tailed, and ligated with a full-length adapter for further PCR amplification. PCR products were purified (AMPure XP system), and libraries were quantified using real-time PCR after size distribution analysis using an Agilent 2100 Bioanalyzer. Index-coded samples were clustered with a cBot Cluster Generation System according to the manufacturer's instructions. Ultimately, libraries were sequenced to generate 150 bp paired-end reads (HiSeq sequencing platform, Illumina Inc., US). *Metagenome assembly and binning.* The raw shotgun metagenome reads were screened using Trimmomatic v0.36 with the parameters set as follows: *LEADING:3 TRAILING:3 SLIDINGWINDOW:4:15 MINLEN:70* [41]. The trimmed reads were assembled de novo into contigs using metaSPAdes v3.14.0 with default parameters [42]. The trimmed reads were mapped back onto the assembled contigs using the *mem* algorithm implemented in BWA v0.7.17, and the mapping data were sorted using SAMtools v1.10 [43, 44]. The coverage of each contig was calculated using *jgi_summarize_bam_contig_depths* command implemented in MetaBat2 with the parameters *minContigLength* and *minContigDepth* set to 2000 and 2, respectively [45]. These coverage data were used as the input to MetaBat2 for binning the contigs into metagenome assembled genomes (MAG) [45]. CheckM v1.1.2 software was implemented to assess the quality of the bins by computing their completeness and contamination (*lineage_wf* command) [46]. MAGs potentially belonging to a single organism were identified and subsequently merged (*merge* command) after manually inspecting their marker gene sets and coverage information [46]. The bins were subsequently refined using refineM, removing the contigs violating consistency in terms of contig statistics (computed with *scaffold_stats* command) and/or taxonomic affiliations of the protein-coding sequences within [47]. Protein-coding sequences were also predicted with refine using the *call_genes* command and their taxonomic affiliation was inferred using the *taxon_profile* command with the GTDB database release 80 as reference. Subsequently, inconsistent contigs were identified with the *taxon_filter* and removed. After filtering out all potential outlier contigs, the bins were further filtered with the completeness and contamination thresholds set to 75% and 5%, respectively. *Metagenome annotation.* The taxonomy affiliations of the refined MAGs were inferred using GTDB-tk v2.3.2 with GTDB database release 214 [48]. To estimate the relative abundances of the organisms represented by the MAGs, the quality-trimmed raw reads were mapped onto the contigs in the finalized MAGs using BWA MEM v0.7.17 with default parameters [43]. The alignment files were sorted with SAMtools v1.10, and the coverages of the contigs in the MAGs were calculated using *coverage* command of checkM v1.1.2 [46]. The relative abundance of each MAG was calculated using *profile* command and represented as the percentage of total reads mapped to the contigs in the MAG, normalized by the total size of the contigs in the MAG. The potential coding sequences within each MAG were annotated using MetaErg v1.2.0 with Pfam, TIGRFAMS, Metabolic-hmms, SwissProt, and RefSeq databases as reference [49]. Annotation was supplemented with Ghostkoala [50]. The functions, domain structures, KEGG Orthology (KO) numbers, Gene Orthology numbers (GO), and Enzyme Commission numbers (EC) were included in the annotation. The annotation of the two *nosZ* clades was manually refined on Interpro [51] based on the twin-arginine translocation (clade I, IPR006311) or the general secretory (clade II, IPR026468) pathway-specific signal peptides [52]. The cobalamin-dependent epoxyqueuosine reductase *queG* (EC 1.17.99.6), and its cobalamin-independent functional homolog *queH* [53], were differentiated phylogenetically using annotated *queG* and *queH* sequences from UniProtKB [54]. The same approach was used to differentiate the two nucleotide loop assembly marker genes for cobalamin production, *cobP*, *cobU*, and *cobY*. The software Anvi'o v.8 was used to align concatenated ribosomal genes identified across MAGs, and the phylogenetic tree was built from the alignment using FastTree (Fig. S2).

### Mass spectrometry based proteomics [55, 56]

*Protein extraction and proteolytic digestion. Protein extraction.* Approximately 25 mg of biomass (wet weight) was collected in an Eppendorf tube and solubilized in a suspension buffer consisting of 175 $\mu$L B-PER reagent (Thermo Scientific) and 175 $\mu$L TEAB buffer (50 mM TEAB, 1% (w/w) NaDOC, adjusted to pH 8.0). Next, 0.1 g of glass beads (acid-washed, approximately 100 $\mu$m in diameter) were added and the cells were disrupted using 5 cycles of bead beating on a vortex for 1 min, followed by cooling on ice for 30 s. Then, a freeze/thaw step was performed by freezing the suspension at −80°C for 20 min, and thawing it while shaking in an incubator. The cell debris was pelleted at 14000 × g for 10 min while being cooled at 4°C. The supernatant was transferred to a new Eppendorf tube. *Protein precipitation.* The protein was precipitated by adding 1 volume of TCA (trichloroacetic acid) to 4 volumes of the supernatant. The solution was then incubated at 4°C for 10 min and pelleted again at 14000 × g for 10 min. The resulting protein pellet was washed twice with 200 $\mu$L of ice-cold acetone. *Trypsin digestion.* The protein pellet was dissolved in 200 mM ammonium bicarbonate containing 6 M urea to achieve a final concentration of approximately 100 $\mu$g/$\mu$L. To 100 $\mu$L of the protein solution, 30 $\mu$L of a 10 mM DTT solution was added and incubated at 37°C for 1 h. Next, 30 $\mu$L of a freshly prepared 20 mM IAA solution was added and incubated in the dark for 30 min. The solution was then diluted to a concentration of <1 M Urea using a 200 mM ammonium bicarbonate buffer, and an aliquot of approximately 25 $\mu$g of protein was digested with Trypsin (Promega, Trypsin to protein ratio of 1:50) at 37°C overnight. *Solid phase extraction.* The peptides were desalted using an Oasis HLB 96-well plate (Waters) as per the manufacturer's instructions. The purified peptide eluate was then dried using a speed vac concentrator. *Large-scale shotgun proteomics and label-free quantification.* An aliquot containing approximately 250 ng protein digest was analysed in duplicates using an one-dimensional shotgun proteomics approach. Each duplicate was injected twice. Briefly, the samples were analysed using a nano-liquid-chromatography system consisting of an EASY nano-LC 1200, equipped with an Acclaim PepMap RSLC RP C18 separation column (50 $\mu$m × 150 mm, 2 $\mu$m), and an QE plus Orbitrap mass spectrometer (Thermo Scientific, Germany). The flow rate was maintained at 350 nL/min. Following sample loading and a wash step at 5% B, a linear gradient was performed, first to 25% B over 88 min, and further to 50% B over additional 25 min. Finally, the separation column was back equilibration to starting conditions. Solvent A was $H_2O$ containing 0.1% formic acid, and solvent B consisted of 80% acetonitrile in $H_2O$ and 0.1% formic acid. The spectrometer was operated in the data dependent acquisition mode, thereby measuring peptide signals from the 385–1250 m/z range at 70 K resolution with the AGC target of 3e6 and max IT of 100 ms. The top 10 signals were isolated at a window of 2.0 m/z and fragmented using a NCE of 28. Fragments were acquired at 17 K resolution, at an AGC target of 5e4 and 100 ms max IT. *Database searching, comparison of conditions, and data visualization.* Data were analysed using a database of *in silico* translated gene-coding sequences obtained from shotgun metagenome experiments of the analysed enrichment cultures (as described above) with PEAKS Studio 10 (Bioinformatics Solutions Inc, Canada). Database searching was performed by allowing for 20 ppm parent ion mass error tolerance and 0.02 m/z fragment ion mass error tolerance and allowing of up to 2 missed cleavages. Carbamidomethylation was set as fixed modification and methionine oxidation and N/Q deamidation were considered as variable modifications. Peptide spectrum matches were filtered against 1% false discovery rate (FDR) and protein identifications with ≥2 unique peptides were considered as significant identifications. The relative abundance of each protein is presented in terms of normalized spectral counts, defined as spectral counts per protein divided by its molecular weight, and divided by the sum of spectral counts of the specific injection. Only proteins identified in at least two out of four injections were included in the analysis, and the average of their normalized spectral counts in the different injections is taken as proxy for their relative abundance. RStudio v2023.03.1 [57] with R v4.3.0 [58] was used for data analysis and visualization.

### Amplicon sequencing

Biomass samples were collected on a weekly basis for 16S rRNA gene amplicon sequencing. The protocols for DNA extraction, sequencing, and data processing and analysis, are detailed in Fig. S3 in the Supporting Information. The resulting microbial composition profiles at Family level are also presented therein.

## Results and discussion

### Reduced biomass growth under continuous $N_2O$ excess

Two $N_2O$-respiring mixed cultures were successfully enriched in a chemostat over multiple generations with acetate and $N_2O$ as sole electron donor and acceptor, respectively (Fig. 1; Table S1). Acetate (*$N_2$Oexc*) and $N_2O$ (*$N_2$Olim*) limiting conditions were imposed to assess the impact of substrate affinity on community assembly at low dilution rates. Specifically, the imposed dilution rate was almost five times lower than previously applied in non-axenic $N_2O$-reducing chemostat works [29]. Both enrichments featured lower biomass growth yields on $N_2O$ ($Y_{X/N2O}$) and acetate ($Y_{X/Ac}$) compared to those obtained by [29] with an identical set-up and comparable operating conditions with the exception of the ultrafiltration membrane used in this study (Table 1). The observed lower yields are consistent with greater relative allocation of resources to maintenance at lower growth rates. The stoichiometric consumption of 3.1–3.4 moles $N_2O$ per mole acetate consumed was slightly higher than the values obtained by [29] (Table 1). The yields of ammonium consumed per biomass produced ($Y_{NH4/X}$) were higher than expected for the commonly assumed empirical biomass composition ($CH_{1.8}O_{0.5}N_{0.2}$ [38]), yet comparable to the ones of the *Pseudomonas stutzeri* JM300 strain grown on $N_2O$ and acetate [29].

Importantly, the growth yields on both $N_2O$ and acetate were substantially lower in *$N_2$Oexc* than in *$N_2$Olim* (Table 1). This is in agreement with [29], and likely relates to the potential cytotoxic effects of $N_2O$ [33, 59, 60]. Based on average off-gas $N_2O$ concentrations, the estimated dissolved $N_2O$ concentration in *$N_2$Oexc* was 382 ± 25 $\mu$M, exceeding by far the concentration at which cytotoxic effects have been previously reported [60]. The estimated biomass-specific acetate consumption rate for maintenance was 2.4-fold higher under $N_2O$ excess (0.019 ± 0.001 C-$mol_{Ac}{\cdot}mol_X^{-1}{\cdot}h^{-1}$) than when $N_2O$ was limiting (0.008 ± 0.001 C-$mol_{Ac}{\cdot}mol_X^{-1}{\cdot}h^{-1}$). This further supports the negative impact of $N_2O$ on growth.

### *Rhodocyclaceae*-dominated $N_2O$-respiring enrichments

To resolve the identity and metabolic potential of the enriched organisms we sequenced the metagenomes of the two steady-state cultures. A total of $75.2{\cdot}10^6$ and $64.5{\cdot}10^6$ reads (*$N_2$Oexc* and *$N_2$Olim*, respectively) were obtained after quality filtering, and their assembly yielded 6550 and 7001 contigs (> 2000 bp) with

**Table 1.** Biomass, ammonium, and $N_2O$ stoichiometric yields of the *$N_2$Oexc* and *$N_2$Olim* enrichments. Values were calculated based on the measured consumption and production rates after data reconciliation (days 100–150 for *$N_2$Oexc* and 60–100 for *$N_2$Olim*; Table S1), and standard deviations were estimated by propagating the relative error of each measured rate. The yields obtained by [29] at higher dilutions with an identical set-up, used for the estimation of the biomass-specific substrate consumption rate for maintenance, are also presented. Stoichiometrically, 4 moles of $N_2O$ are required to respire 1 mole of acetate.

| D $h^{-1}$ | $N_2O$/Ac (inf.) mol/mol | $Y_{X/Ac}$ $mol/mol_C$ | $Y_{X/N2O}$ mol/mol | $Y_{N2O/Ac}$ mol/mol | $Y_{NH4/X}$ mol/mol | |
|---|---|---|---|---|---|---|
| 0.006 ± 0.001 | 12.8 ± 1.5 | 0.15 ± 0.03 | 0.09 ± 0.02 | 3.42 ± 0.35 | 0.41 ± 0.15 | **$N_2$Oexc** |
| 0.028 ± 0.001 | 15.9 | 0.25 ± 0.02 | 0.16 ± 0.01 | 3.06 ± 0.2 | 0.28 ± 0.02 | Conthe et al. 2018c |
| 0.089 ± 0.003 | 26.1 | 0.27 ± 0.01 | 0.17 ± 0.01 | 3.1 ± 0.17 | 0.28 ± 0.01 | Conthe et al. 2018c |
| 0.006 ± 0.001 | 1.8 ± 0.1 | 0.24 ± 0.04 | 0.15 ± 0.03 | 3.1 ± 0.15 | 0.44 ± 0.13 | **$N_2$Olim** |
| 0.027 ± 0.001 | 2.3 | 0.32 ± 0.04 | 0.22 ± 0.04 | 2.86 ± 0.51 | 0.26 ± 0.01 | Conthe et al. 2018c |
| 0.086 ± 0.003 | 2.7 | 0.33 ± 0.03 | 0.26 ± 0.02 | 2.49 ± 0.29 | 0.25 ± 0.02 | Conthe et al. 2018c |

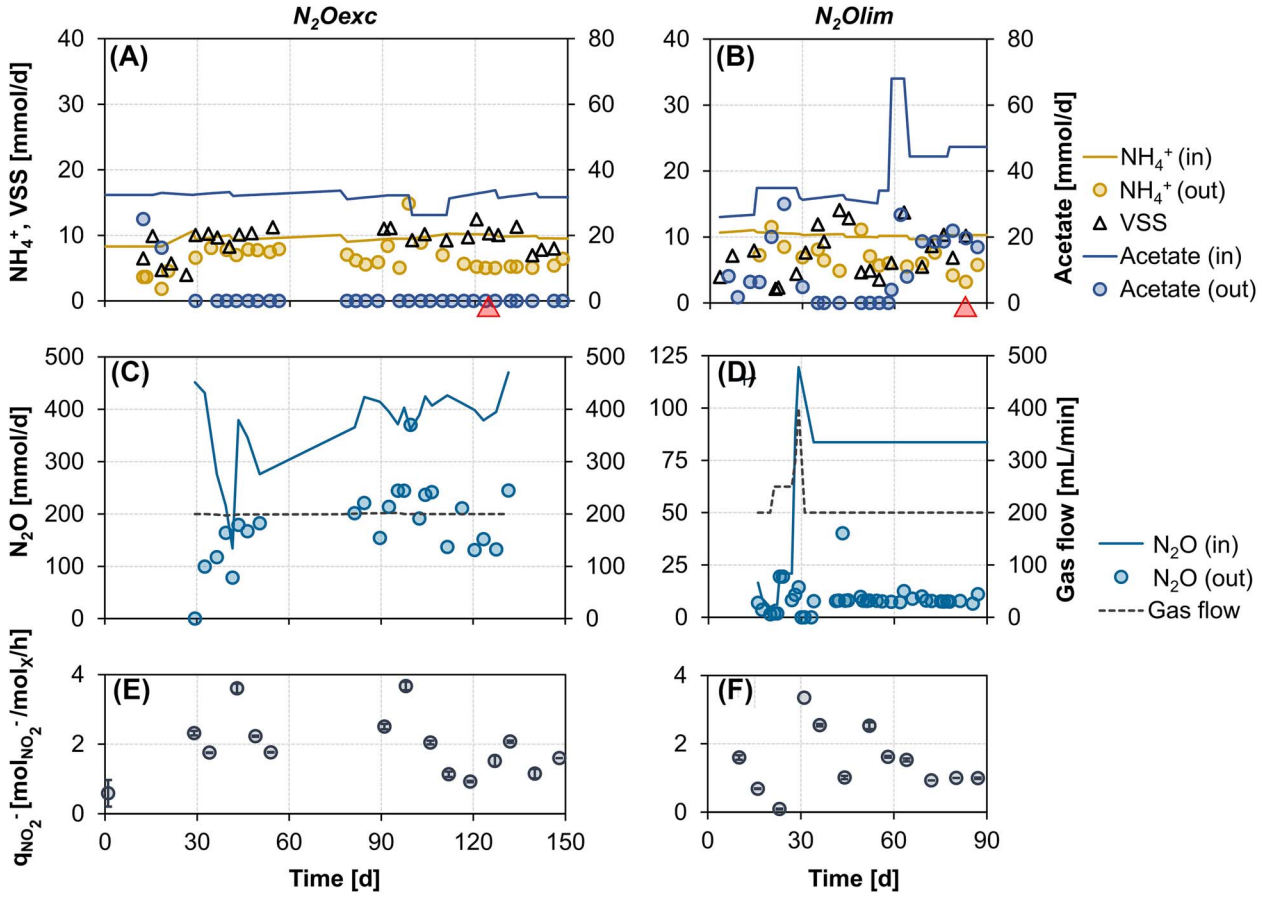


**Figure 1.** Overall and biomass specific performance of the two cultures enriched under excess (*$N_2$Oexc*) and limiting (*$N_2$Olim*) availability of nitrous oxide as sole electron donor. (A and B) Influent and effluent acetate and ammonium rates, and biomass production rate. *Full triangle*: day of biomass sampling for metagenomic and metaproteomic analysis. (C and D) influent and effluent $N_2O$ rates, and imposed gas flow. (E and F) *Ex-situ* maximum biomass specific $NO_2^-$ consumption rate.

N50 values of $18.8{\cdot}10^3$ and $12.6{\cdot}10^3$ bp. Contigs were binned, resulting in 10 and 17 metagenome-assembled genomes (MAGs), with completeness >75% and contamination <5% (Table 2). The recovered MAGs accounted for 94.5 and 74.1% of the quality-filtered reads in *$N_2$Oexc* and *$N_2$Olim*, respectively. The obtained binning coverage indicates that the recovered MAGs represent the majority of the two microbiomes. In terms of relative reads abundance, AZO_exc (*$N_2$Oexc*) and AZO_lim (*$N_2$Olim*) were the dominant MAGs, and accounted for about 83.2 and 67.1% of the reads in the respective reactors. Low quality MAGs were grouped with the unbinned reads (Table 2).

Beyond the genetic fingerprints of the two cultures, we analysed the proteomes of the same samples to quantify the relative biomass contribution and infer the actual metabolic role of each microorganism represented by a MAG [61]. Per sample, an average of 20 981 and 16 832 MS2 spectra (*$N_2$Oexc* and *$N_2$Olim*, respectively) was obtained over quadruplicate injections. We identified an average of 14 490 and 12 449 peptides, resulting in 1613 and 1324 proteins identified with a FDR < 0.01 by at least 2 unique peptides in at least 2 out of 4 injections. The relative abundance of a protein was calculated by dividing its normalized spectral counts by the sum of the normalized spectral counts in the corresponding

**Table 2.** Genomic and proteomic characteristics of the recovered MAGs. MAGs marked with (*) affiliate with the *Rhodocyclaceae* family. MAGs marked with (‖) or (‡) share a genome-aggregate average nucleotide identity (ANI) > 99%.

| | | Metagenome | | | | | | | | Metaproteome | | |
|---|---|---|---|---|---|---|---|---|---|---|---|---|
| | Bin ID | Complet. | Contam. | Bin size [Mbp] | N50 [bp] | GC [%] | Mapped reads | Mapped reads [%] | Predicted proteins | Detected proteins | Rel. abund. spectra [%] | Taxonomy |
| ***N₂Oexc*** | **AZO_exc*** | 97.6 | 0.0 | 2.7 | 171 993 | 59.8 | 62 591 220 | 83.2 | 2614 | 1077 | 75.8 | Genus *Azonexus* |
| | **Bin.2_exc** | 94.5 | 0.4 | 3.2 | 49 531 | 60.5 | 1 470 411 | 2.0 | 3009 | 143 | 5.4 | Genus *Phaeovulum* |
| | **Bin.24_exc** | 97.5 | 0.5 | 3.3 | 33 922 | 59.3 | 1 160 565 | 1.5 | 3023 | 117 | 5.1 | Genus *Pseudorhodobacter* |
| | **Bin.15_exc** | 98.2 | 0.0 | 3.5 | 133 854 | 46.6 | 4 181 484 | 5.6 | 3299 | 98 | 3.7 | Genus *Bdellovibrio* |
| | **Bin.3_exc** | 77.8 | 1.8 | 3.1 | 20 050 | 65.3 | 328 268 | 0.4 | 3014 | 20 | 0.8 | Genus *Aquamicrobium* |
| | **Bin.12_exc** | 98.9 | 0.1 | 3.1 | 74 431 | 33.7 | 245 691 | 0.3 | 2787 | 6 | 0.3 | Species *Flavobacterium filum* |
| | **Bin.18_exc‖** | 99.5 | 0.0 | 2.7 | 81 605 | 40.4 | 547 907 | 0.7 | 2424 | 8 | 0.3 | Genus *Moheibacter* |
| | **Bin.16_exc** | 99.0 | 0.0 | 2.5 | 57 459 | 37.3 | 213 672 | 0.3 | 2262 | 8 | 0.2 | Genus *Kaistella* |
| | **Bin.17_exc** | 99.0 | 0.0 | 2.9 | 65 957 | 39.2 | 241 612 | 0.3 | 2480 | 3 | 0.1 | Genus *Ferruginibacter* |
| | **Bin.9_exc‡** | 95.8 | 0.5 | 2.5 | 13 365 | 35.0 | 131 267 | 0.2 | 2281 | - | 0.0 | Genus *Ferruginibacter* |
| | ***Unbinned*** | - | - | 26.4 | 5341 | - | 4 099 244 | 5.5 | 27 394 | 133 | 8.4 | - |
| ***N₂Olim*** | **AZO_lim*** | 87.3 | 0.0 | 2.7 | 32 281 | 63.5 | 43 300 280 | 67.1 | 2492 | 648 | 50.8 | Genus *Azonexus* |
| | **THA_lim*** | 100.0 | 0.7 | 4.2 | 38 798 | 69.5 | 1 247 092 | 1.9 | 3747 | 181 | 13.5 | Species *Thauera phenylacetica* |
| | **Bin.14_lim‖** | 77.2 | 0.1 | 2.0 | 4921 | 40.5 | 78 531 | 0.1 | 2090 | 43 | 2.1 | Family *Weeksellaceae* |
| | **Bin.21_lim‡** | 99.5 | 0.3 | 2.6 | 104 725 | 35.2 | 520 671 | 0.8 | 2170 | 60 | 1.8 | Genus *Ferruginibacter* |
| | **Bin.6_lim** | 75.4 | 1.8 | 2.5 | 24 195 | 48.9 | 243 575 | 0.4 | 2366 | 17 | 0.7 | Species *Seleniivibrio woodruffii* |
| | **Bin.24_lim** | 78.0 | 1.1 | 1.3 | 57 096 | 24.0 | 486 035 | 0.8 | 1137 | 12 | 0.5 | Phylum *Patescibacteria* |
| | **Bin.20._lim*** | 76.9 | 0.9 | 3.1 | 6309 | 66.0 | 141 837 | 0.2 | 3184 | 7 | 0.4 | Species *Azovibrio restrictus* |
| | **Bin.26_lim** | 89.8 | 3.9 | 2.4 | 13 434 | 61.7 | 134 723 | 0.2 | 2332 | 1 | 0.2 | Genus *Pseudoflavonifractor* |
| | **Bin.11_lim** | 93.0 | 1.6 | 3.9 | 17 980 | 43.9 | 214 463 | 0.3 | 3203 | 6 | 0.1 | Order *Bacteroidales* |
| | **Bin.2_lim** | 93.5 | 0.1 | 1.7 | 11 915 | 50.4 | 233 247 | 0.4 | 1697 | 4 | 0.1 | Family *Anaerovoracaceae* |
| | **Bin.8_lim** | 78.5 | 2.8 | 2.6 | 4471 | 38.0 | 101 235 | 0.2 | 2495 | 3 | 0.1 | Genus *Niabella* |
| | **Bin.10_lim** | 93.7 | 1.1 | 2.9 | 42 970 | 33.1 | 262 567 | 0.4 | 2266 | 3 | 0.1 | Order *Bacteroidales* |
| | **Bin.1_lim** | 76.2 | 0.1 | 1.1 | 4590 | 37.2 | 43 318 | 0.1 | 1208 | 1 | 0.1 | Genus *Paracholeplasma* |
| | **Bin.27_lim** | 81.2 | 1.9 | 3.4 | 6337 | 37.4 | 142 977 | 0.2 | 3430 | 1 | 0.0 | Genus *Fusibacter_C* |
| | **Bin.23_lim** | 96.2 | 1.1 | 2.4 | 106 442 | 31.2 | 461 252 | 0.7 | 1972 | 3 | 0.0 | Order *Bacteroidales* |
| | **Bin.22_lim** | 79.2 | 1.1 | 1.3 | 5309 | 41.6 | 53 843 | 0.1 | 1457 | - | 0.0 | Family *Erysipelotrichaceae* |
| | **Bin.18_lim** | 97.3 | 0.0 | 2.4 | 37 598 | 34.4 | 140 114 | 0.2 | 2000 | - | 0.0 | Family *Paludibacteraceae* |
| | ***unbinned*** | - | - | 14.9 | 5762 | - | 16 727 548 | 25.9 | 15 000 | 334 | 29.5 | - |

injection. About 91.7 and 74.7% of the proteins identified in *N₂Oexc* and *N₂Olim*, respectively, were mapped to the recovered MAGs, providing a comprehensive coverage of the expressed functional potential of the enrichments. AZO_exc and AZO_lim accounted for 70.1 and 50.6% of their respective metaproteome, consistent with their metagenomic-based relative abundance (Table 2). In contrast, THA_lim, that represented only 1.9% of the metagenomic reads in *N₂Olim*, accounted for 14.0% of the metaproteome, suggesting a more prominent metabolic role than predicted based on the sole metagenome. Moreover, for the three dominant MAGs we identified 1077 (AZO_exc), 648 (AZO_lim), and 181 (THA_lim) proteins representing the 41.2, 26.0, and 4.8% of their respective metagenome-predicted coding genes.

Taxonomically, the recovered draft genomes were affiliated to the phyla *Bacteroidota* (*Bacteroidetes*; 12), *Pseudomonadota* (*Proteobacteria*; 7), *Bacillota (Firmicutes;* 5), *Bdellovibrionota* (1), *Patescibacteria* (1), and *Deferribacterota* (1) (Table 2; Table S2). All three dominant MAGs (AZO_exc, AZO_lim, and THA_lim) affiliated with the family *Rhodocyclaceae*, and shared an average nucleotide identity <84% indicating that they do not belong to the same species [62] (see Table S2). AZO_exc and AZO_lim affiliated with the genus *Azonexus*, while THA_lim with the genus *Thauera*. The selectivity of the imposed conditions is further supported by 16S rRNA gene-based amplicon sequencing (Fig. S3). A single OTU affiliated with the *Rhodocyclaceae* family, initially present at very low relative reads abundances in the inoculum (< 1%), was progressively enriched in *N₂Oexc*. The OUT reached steady-state relative abundances between 55 and 70%, in strong agreement with the AZOexc abundance in the metagenome. Two OTUs affiliated with the *Rhodocyclaceae* family dominated *N₂Olim*, consistently with the steady-state metagenomic coexistence of AZO_lim and THA_lim. Globally, the microbially diverse and metabolically versatile *Rhodocyclaceae* family constitutes a core taxon in WWTP microbiomes, driving denitrification and likely $N_2O$ reduction across diverse ecosystems [9, 12, 63–65]. *Rhodocyclaceae* members are also commonly co-enriched based on their $N_2O$ reducing capability under non-axenic conditions in chemostats [28, 29, 66, 67] and biofilm-based systems [15]. Within the *Rhodocyclaceae* family, *Azonexus* genus affiliates have recently been enriched and isolated from biogas digestate, and their catabolic preference for $N_2O$ reduction has been shown both at kinetic and proteomic level [68]. Our study further supports the prominent role of *Rhodocyclaceae* family members in providing a potential $N_2O$ sink in diverse ecosystems.

## High-affinity clade II $N_2O$-reducers selected under $N_2O$ limitation and low biomass dilution rates

We interrogated the recovered MAGs for genes and proteins involved in the reduction of nitrogen oxides. Consistently with

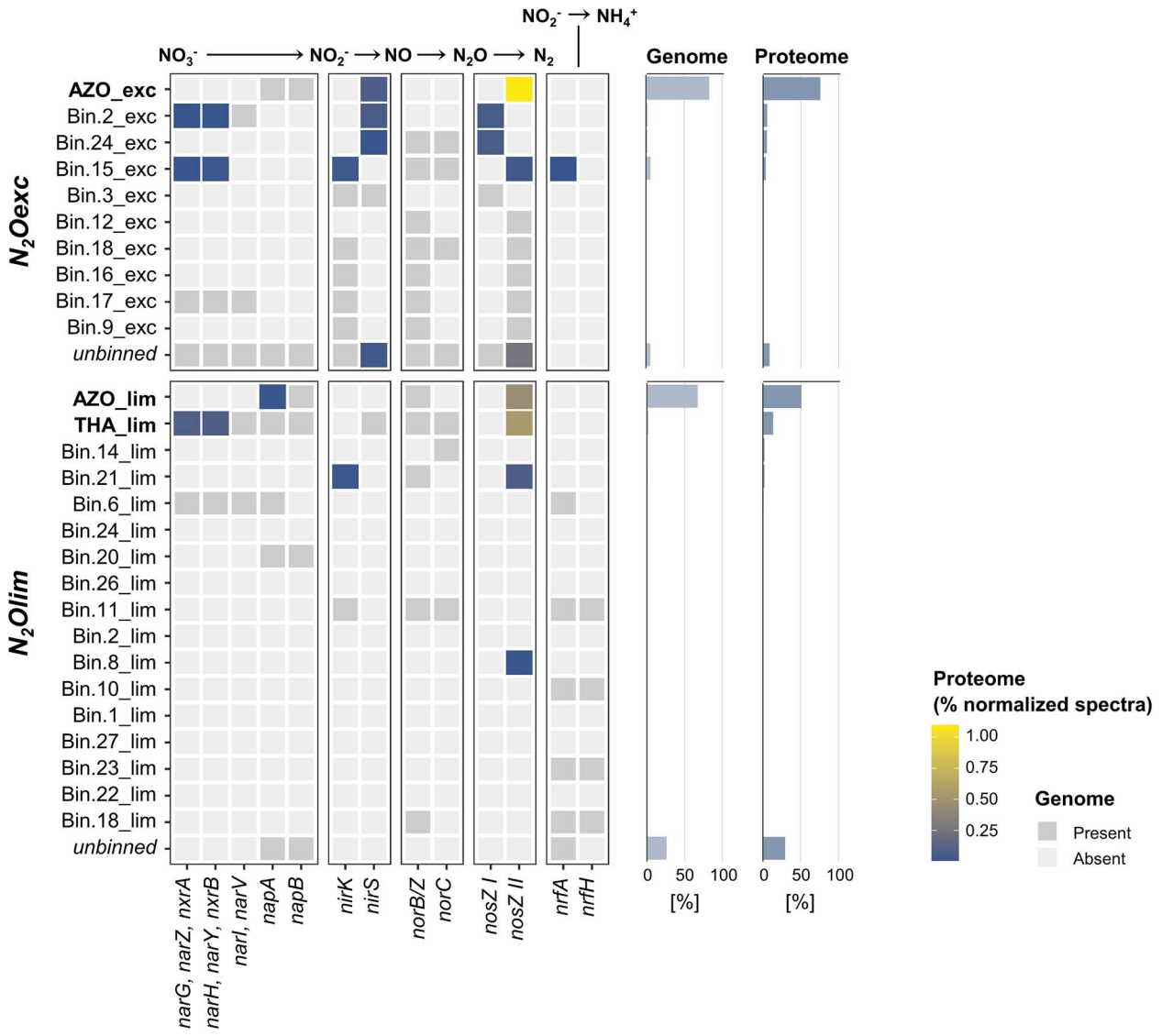


**Figure 2.** Denitrification and dissimilatory nitrite reduction to ammonium (DNRA). Gene presence (dark grey tiles) and protein abundance (colored tiles) for the high- and medium-quality (completeness >75% and contamination <5%) MAGs enriched under excess ($N_2Oexc$) and limiting ($N_2Olim$) nitrous oxide availability. The sum of the normalized spectral counts for each protein was taken as a proxy for protein abundance. Right bar charts: relative abundance of each MAG in the metagenome (based on relative reads alignment) and the metaproteome (summed relative abundance of normalized spectral counts of peptides matching to predicted proteins in each MAG). Abbreviations: *napAB*: Electron transfer (*napB*; EC:1.9.6.1; K02567) and catalytic (*napA*; K02568) subunits of the periplasmic nitrate reductase. *narGHI*: membrane-bound nitrate reductase, comprising the transmembrane protein *narI* (EC:1.7.5.1, 1.7.99.-; K00374) mediating the electron transfer from the quinol pool via *narH* (EC:1.7.5.1, 1.7.99.-; K00371) to the catalytic subunit *narG* (EC:1.7.5.1, 1.7.99.-; K00370). *nirK*: copper-containing nitrite reductase (EC:1.7.2.1; K00368). *nirS*: cytochrome $cd_1$-containing nitrite reductase (EC:1.7.2.1, 1.7.99.1; K15864). *norCB*: nitric oxide reductase comprising the two subunits *norC* (K02305) and *norB/Z*; the latter comprises both the cytochrome c-dependent (*cNorB*; EC:1.7.2.5; K04561) and the menaquinol-dependent (*qNorB/NorZ*; EC:1.7.5.2) variants [68]. *nrfAH*: catalytic (*nrfA*; EC:1.7.2.2; K03385) and electron donating (*nrfH*; K15876) subunits of the periplasmic dissimilatory cytochrome c nitrite reductase.

nitrous oxide being the sole electron acceptor, the nitrous oxide reductase (NosZ) was among the ten most abundant proteins with an assigned KO number in $N_2Oexc$ and $N_2Olim$, accounting for 1.4 and 1.1% of the total normalized spectral counts respectively (Fig. 2; Table S2). All recovered MAGs under $N_2O$ excess possessed a *nosZ* gene. AZO_exc harbored genes encoding for the clade II NosZ protein, and contributed the most to its overall expression (Fig. 2). Clade I harboring genomes were also present in $N_2Oexc$, albeit at very low relative abundances (Fig. 2). The co-existence of the two clades aligns with the majority of characterized natural communities [4, 69] and $N_2O$-respiring enrichments [15, 26, 27, 29, 67], and suggests that the imposed conditions were not selective enough to fully outcompete clade I $N_2O$-reducers. In contrast, $N_2O$ limitation resulted in the complete washout of the clade I $N_2O$-respiring microorganisms initially present in the inoculum (i.e. $N_2Oexc$), as further confirmed by the absence of the clade I *nosZ* gene sequence even within the unbinned reads (Fig. 2). The NosZ protein belonging to the most abundant AZO_lim and THA_lim shared about 80% of sequence identity with the NosZ of AZO_exc ($N_2Oexc$). Overall, while clade II $N_2O$-reducers clearly played a primary role in both enrichments, to the best of our knowledge $N_2Olim$ constitutes the first enrichment of sole clade II *nosZ* harboring organisms in mixed microbial communities.

Contrary to our expectations, in terms of other reductases, all *nosZ* encoding genomes were not specialist $N_2O$-reducers and possessed at least another nitrate or nitrite reductase gene. Clade II *nosZ* was annotated alone only in the low-abundant medium-quality (76.4% completeness) Bin.8_lim (Fig. 2). The periplasmic

nitrate reductase (*napAB*) was encoded by all three dominant MAGs (AZO_exc, AZO_lim, THA_lim), while only THA_lim also possessed the membrane-bound dissimilatory nitrate reductase *narGHI*. In agreement with published denitrifiers genomes [9], MAGs possessing the cytochrome $cd_1$-type nitrite reductase (*nirS*) did not encode the copper-containing nitrite reductase (*nirK*), and vice versa, with the only exception of the low-abundant Bin.3_exc encoding both (*$N_2$Oexc*). Yet, none of the *nir* was annotated in AZO_lim (*$N_2$Olim*). In contrast to often observed co-occurrence patterns [4, 9], no evident correlation emerged between the presence of *nirS* and *nosZ*, or the nitric oxide reductase (*cNorB* or *qNorB*). The ammonification potential, identified by the presence of the periplasmic energy-conserving periplasmic cytochrome c nitrite reductase *nrfAH* complex, was almost exclusively restricted to the $N_2O$-limiting conditions with acetate excess (*$N_2$Olim*), in an interesting parallel with the electron donor-rich environments selecting for ammonifiers [70]. Despite $N_2O$ being the only electron acceptor, some NarG/NapA and NirK/NirS enzymes were detected in the proteome, yet at more than one order of magnitude lower abundances than NosZ (Fig. 2). The observed constitutive expression of the denitrifying enzymes is consistent with the significant maximum *ex-situ* nitrite reduction capacity maintained in both enrichments (Fig. 1) in analogy to [29] and [25].

Taken together, our results suggest that $N_2O$ limiting conditions at sufficiently low growth rates (here 0.006 $h^{-1}$) exclusively select for *clade II* $N_2O$-reducers. To date, this was only hypothesized based on the higher affinity displayed by a limited number of characterized clade II isolates [15, 16], and the positive correlation between clade II *nosZ* gene abundance and long retention times reported in the work of Conthe and colleagues [28, 29]. Follow-up research should target the independent experimental confirmation of our findings and the currently elusive conditions that further select for non-denitrifying specialist $N_2O$-reducers in natural and engineered microbiomes.

## Cobalamin auxotrophy as potential competitive advantage at high $N_2O$

We hypothesize that the cytotoxic effects of elevated $N_2O$ levels in the growth medium led to the observed lower growth yields in *$N_2$Oexc*, and shaped the corresponding community assembly. $N_2O$ is known to selectively inactivate cobalamin (vitamin $B_{12}$), an essential cofactor in bacterial metabolism [33, 59]. High $N_2O$ concentrations have been shown to hinder microbial growth by compromising the activity of cobalamin-dependent enzymes [60]. Cobalamin synthesis itself constitutes a significant genetic and metabolic burden for the cell, involving up to thirty enzymes [71], and in environmental communities it is usually performed by a small cohort of prototrophic low-abundant microorganisms [72, 73]. In this perspective, genes encoding proteins involved in cobalamin synthesis and transport, and in core cobalamin-dependent metabolic pathways were searched for in the recovered MAGs.

We identified AZO_exc (*$N_2$Oexc*) and THA_lim (*$N_2$Olim*) as de novo cobalamin producers based on the presence of seven of the eight experimentally-verified biosynthetic marker genes proposed by [73] (corrin ring biosynthesis: *cbiL/cobI*, *cbiF/cobM*, *cbiC/cobH*; nucleotide loop assembly: *cobQ/cbiP*, *cobC1/cobC/cbiB/cobD*, *cobS/cobV*, and *cobP/cobU*, except *cobY*; Fig. 3, Table S3). The entire cobalamin production pathway was also almost completely annotated in both MAGs, and the majority of predicted proteins were detected in AZO_exc. In contrast, AZO_lim (*$N_2$Olim*) contained all nucleotide loop assembly steps, but lacked two of the downstream corrin ring biosynthetic marker genes, namely *cbiL/cobI* and *cbiC/cobH*, along with a more inconsistent pathway annotation (Fig. 3). On these grounds, while missing annotations e.g. due to the lower MAG completeness (87.3%) or non-homologous replacements cannot be ruled out, AZO_lim seems to have relied on the uptake of late cobalamin intermediates (e.g. cobinamide) either from the yeast extract present in the influent or produced by THA_lim [73]. The high protein expression of the outer membrane cobalamin/cobinamide transporter (BtuB; [71, 72]) in both MAGs further supports this hypothesis (Fig. 3). Conversely, in *$N_2$Oexc*, AZO_exc was devoid of the vitamin B12 transporter gene *btuB*, and the BtuB protein was detected at low abundances only in side populations.

Both enrichments encoded the cobalamin-dependent processes most widely found in bacterial genomes, encompassing amino acid and nucleotide synthesis [72, 73]. All three dominant MAGs possessed the cobalamin-dependent methionine synthase (*metH*), while AZO_lim encoded also its cobalamin-independent orthologue (*metE*; Fig. 3). *metE* has been previously shown to be up-regulated under cobalamin-limiting conditions, e.g. at high $N_2O$, albeit displaying significantly lower activities [60]. Yet, only the cobalamin-dependent MetH was detected in the proteome of AZO_lim. The reliance of all three MAGs on vitamin B12 was further supported by the presence of the cobalamin-dependent epoxyqueuosine reductase (*queG*), involved in tRNA modification, and by the expression of methylmalonyl CoA mutase (*MUT*), catalyzing the synthesis of succinyl-CoA [74].

We suggest that de novo cobalamin production provided AZO_exc with a selective advantage in *$N_2$Oexc*. High $N_2O$ concentrations likely compromised both the internal and exogenous (i.e. from yeast extract) active vitamin B12 pool, making cobalamin self-sufficiency an essential metabolic trait. Conversely, the more permissive conditions in *$N_2$Olim* made cobalamin cross-feeding viable, and its production dispensable [75]. The high expression of the cobalamin transporter (BtuB) may suggest the reliance of both AZO_lim and THA_lim on the uptake of the exogenous yeast extract cobalamin. However, we reason that the genome-inferred cobalamin-prototrophy provided AZO_lim with a higher relative fitness, i.e. allowing for an optimized cellular proteome allocation [76–78], while creating the ecological niche for the unexpected co-enrichment of the putative cobalamin-producer THA_lim. Overall, the abundances of the corresponding proteins were relatively low especially in the *$N_2$Olim* (Fig. 3), in line with reported low detections of cobalamin production gene-transcripts even in cobalamin-free cultures [79]. While caution is warranted in their interpretation, and pending direct experimental confirmation, the higher detection of cobalamin synthesis proteins in *$N_2$Oexc* compared to *$N_2$Olim* (Fig. 3) further emphasizes an increased need to sustain an otherwise continuously compromised cobalamin pool. Ultimately, our genome-resolved metaproteome-based evidence suggests that cobalamin cross-feeding may partially underpin the often reported coexistence of $N_2O$ reducers in natural and engineered complex ecosystems.

## Acknowledgements

The authors are deeply indebted to Dimitry Sorokin (TU Delft) for the thorough discussions and invaluable insights.

## Author contributions

Michele Laureni (Conceptualization, Methodology, Software, Validation, Formal analysis, Data curation, Visualization, Supervision, Resources, Funding acquisition, Writing—original draft), Francesc Corbera Rubio (Conceptualization, Methodology, Investigation,

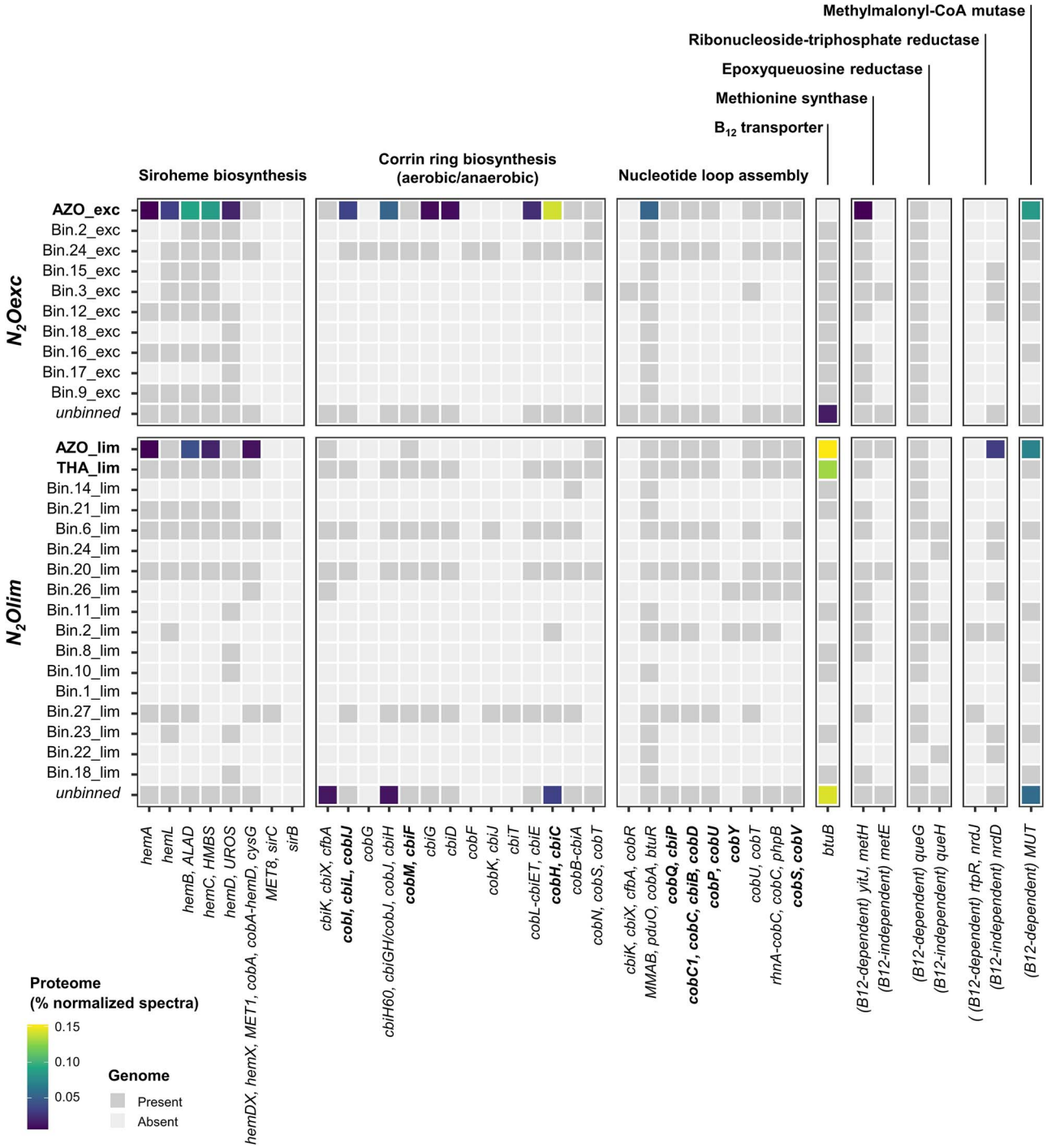


**Figure 3.** Cobalamin bio-synthesis and transport, and cobalamin (in)dependent enzymes. Gene presence (dark grey tiles) and protein abundance (colored tiles) for the high- and medium-quality MAGs enriched under excess ($N_2Oexc$) and limiting ($N_2Olim$) nitrous oxide availability. Annotations: corrin ring biosynthesis (aerobic/anaerobic) marker genes: *cobI*, *cbiL*, *cobIJ* (EC:2.1.1.130, EC:2.1.1.151; K03394, K13540). *cub*, *cbiF* (EC:2.1.1.133, EC:2.1.1.271: K05936). cobH, cbiC (EC:5.4.99.61, EC:5.4.99.60; K06042). Nucleotide loop assembly marker genes: *cobQ*, *cbiP* (EC:6.3.5.10; K02232). *cobC1*, *cobC*, *cbiB*, *cobD* (EC:6.3.1.10; K02225, K02227). *cobP*, *cobU* (EC:2.7.1.156; K02231). *cobS*, *cobV* (EC:2.7.8.26; K02233). *cobY* (EC:2.7.7.62; K19712). Transport and (in)dependent enzymes. *btuB*: cobalamin/cobinamide transporter (K16092). *yitJ*, *metH*: cobalamin-dependent methionine synthase (EC:2.1.1.13, EC:1.5.1.54; K00548, K24042). *metE*: cobalamin-independent methionine synthase (EC:2.1.1.14; K00549). *queG*: cobalamin-dependent epoxyqueuosine reductase (EC:1.17.99.6; K18979). *queH*: cobalamin-independent epoxyqueuosine reductase (EC:1.17.99.6; K09765). *nrdJ*, *rtpR*: cobalamin-dependent ribonucleoside-triphosphate reductase (EC:1.17.4.2; K00524, K00527). *nrdD*: cobalamin-independent ribonucleoside-triphosphate reductase (EC:1.1.98.6; K21636). *MUT*: methylmalonyl CoA mutase (EC:5.4.99.2; K01847). Details for all bio-synthesis genes can be found in Table S3.

Formal analysis, Writing—review & editing), DaeHyun Daniel Kim (Methodology, Software, Validation, Formal analysis, Writing—review & editing), Savanna Browne (Software), Nina Roothans (Software, Validation, Formal analysis, Writing—review & editing), David G. Weissbrodt (Writing—review & editing), Karel Olavaria (Writing—review & editing), Nadieh de Jonge (Writing—review & editing), Sukhwan Yoon (Resources, Writing—review & editing), Martin Pabst (Methodology, Software, Validation, Formal analysis, Data curation, Resources, Writing—review & editing), and Mark C.M. van Loosdrecht (Conceptualization, Supervision, Resources, Writing—review & editing)

## Supplementary material

Supplementary material is available at *ISME Communications* online.

## Conflicts of interest

All authors declare no conflict of interest.

## Funding

ML was supported by a Marie Skłodowska-Curie Individual Fellowship (grant agreement 752992) and a VENI grant from the Dutch Research Council (NWO) (project number VI.Veni.192.252). NR was supported by the Dutch Foundation for Applied Water Research (STOWA) and the waterboards Hoogheemraadschap Hollands Noorderkwartier and Waterschap De Dommel. KO was supported by the joint research program NWO–FAPESP of the Dutch Organization for Scientific Research (NWO) and the Sao Paulo Research Foundation (FAPESP) (code NWO: BBE.2017.013; code FAPESP: 2017/50249-6); and by the SIAM Gravitation Grant (024.002.002) from the Dutch Ministry of Education, Culture and Science (OCW).

## Data availability

Raw DNA reads were deposited on the NCBI Sequence Read Archive and medium- and high-quality MAGs were deposited in Genbank under BioProject PRJNA1054980, with MAG accession numbers SAMN46430372 - SAMN46430381 for *$N_2$Oexc*, and SAMN46430382 - SAMN46430398 for *$N_2$Olim*, in the same order as in Table 2. The 16S rRNA gene amplicon sequencing data can be found under BioProject PRJEB84459. The mass spectrometry proteomics raw data, reference sequence database and database search files have been deposited in the ProteomeXchange consortium database with the dataset identifier PXD030677.

## References

1. Edenhofer O, Pichs-Madruga R, Sokona Y *et al. Working Group III Contribution to the Fifth Assessment Report of the Intergovernmental Panel on Climate Change*. Cambridge, UK, New York, NY, USA: Intergovernmental Panel on Climate Change, 2014.
2. Tian H, Xu R, Canadell JG *et al.* A comprehensive quantification of global nitrous oxide sources and sinks. *Nature* 2020;**586**:248–56. https://doi.org/10.1038/s41586-020-2780-0
3. Thomson AJ, Giannopoulos G, Pretty J *et al.* Biological sources and sinks of nitrous oxide and strategies to mitigate emissions. *Philos Trans R Soc Lond B Biol Sci* 2012;**367**:1157–68. https://doi.org/10.1098/rstb.2011.0415
4. Hallin S, Philippot L, Loffler FE *et al.* Genomics and ecology of novel N2O-reducing microorganisms. *Trends Microbiol* 2018;**26**:43–55. https://doi.org/10.1016/j.tim.2017.07.003
5. Schreiber F, Wunderlin P, Udert KM *et al.* Nitric oxide and nitrous oxide turnover in natural and engineered microbial communities: biological pathways, chemical reactions, and novel technologies. *Front Microbiol* 2012;**3**:372. https://doi.org/10.3389/fmicb.2012.00372
6. Wunderlin P, Mohn J, Joss A *et al.* Mechanisms of N2O production in biological wastewater treatment under nitrifying and denitrifying conditions. *Water Res* 2012;**46**:1027–37. https://doi.org/10.1016/j.watres.2011.11.080
7. Simon J, Klotz MG. Diversity and evolution of bioenergetic systems involved in microbial nitrogen compound transformations. *Biochim Biophys Acta* 2013;**1827**:114–35. https://doi.org/10.1016/j.bbabio.2012.07.005
8. Domingo-Felez C, Smets BF. Modeling denitrification as an electric circuit accurately captures electron competition between individual reductive steps: the activated sludge model-electron competition model. *Environ Sci Technol* 2020;**54**:7330–8. https://doi.org/10.1021/acs.est.0c01095
9. Graf DR, Jones CM, Hallin S. Intergenomic comparisons highlight modularity of the denitrification pathway and underpin the importance of community structure for N2O emissions. *PLoS One* 2014;**9**:e114118. https://doi.org/10.1371/journal.pone.0114118
10. Jones CM, Spor A, Brennan FP *et al.* Recently identified microbial guild mediates soil N2O sink capacity. *Nat Clim Chang* 2014;**4**:801–5. https://doi.org/10.1038/nclimate2301
11. Conthe M, Lycus P, Arntzen MO *et al.* Denitrification as an N2O sink. *Water Res* 2019;**151**:381–7. https://doi.org/10.1016/j.watres.2018.11.087
12. Singleton CM, Petriglieri F, Kristensen JM *et al.* Connecting structure to function with the recovery of over 1000 high-quality metagenome-assembled genomes from activated sludge using long-read sequencing. *Nat Commun* 2021;**12**:2009. https://doi.org/10.1038/s41467-021-22203-2
13. Sanford RA, Wagner DD, Wu Q *et al.* Unexpected nondenitrifier nitrous oxide reductase gene diversity and abundance in soils. *Proc Natl Acad Sci USA* 2012;**109**:19709–14. https://doi.org/10.1073/pnas.1211238109
14. Jones CM, Graf DR, Bru D *et al.* The unaccounted yet abundant nitrous oxide-reducing microbial community: a potential nitrous oxide sink. *ISME J.* 2013;**7**:417–26. https://doi.org/10.1038/ismej.2012.125
15. Suenaga T, Hori T, Riya S *et al.* Enrichment, isolation, and characterization of high-affinity N2O-reducing bacteria in a gas-permeable membrane reactor. *Environ Sci Technol* 2019;**53**:12101–12. https://doi.org/10.1021/acs.est.9b02237
16. Yoon S, Nissen S, Park D *et al.* Nitrous oxide reduction kinetics distinguish bacteria Harboring clade I NosZ from those Harboring clade II NosZ. *Appl Environ Microbiol* 2016;**82**:3793–800. https://doi.org/10.1128/AEM.00409-16
17. Marchant HK, Tegetmeyer HE, Ahmerkamp S *et al.* Metabolic specialization of denitrifiers in permeable sediments controls N2 O emissions. *Environ Microbiol* 2018;**20**:4486–502. https://doi.org/10.1111/1462-2920.14385
18. Bertagnolli AD, Konstantinidis KT, Stewart FJ. Non-denitrifier nitrous oxide reductases dominate marine biomes. *Environ Microbiol Rep* 2020;**12**:681–92. https://doi.org/10.1111/1758-2229.12879

19. Herold M, Martinez Arbas S, Narayanasamy S *et al.* Integration of time-series meta-omics data reveals how microbial ecosystems respond to disturbance. *Nat Commun* 2020;**11**:5281. https://doi.org/10.1038/s41467-020-19006-2
20. Lawson CE, Wu S, Bhattacharjee AS *et al.* Metabolic network analysis reveals microbial community interactions in anammox granules. *Nat Commun* 2017;**8**:15416. https://doi.org/10.1038/ncomms15416
21. Speth DR, In 't Zandt MH, Guerrero-Cruz S *et al.* Genome-based microbial ecology of anammox granules in a full-scale wastewater treatment system. *Nat Commun* 2016;**7**:11172. https://doi.org/10.1038/ncomms11172
22. Torresi E, Gulay A, Polesel F *et al.* Reactor staging influences microbial community composition and diversity of denitrifying MBBRs—implications on pharmaceutical removal. *Water Res* 2018;**138**:333–45. https://doi.org/10.1016/j.watres.2018.03.014
23. Vieira A, Galinha CF, Oehmen A *et al.* The link between nitrous oxide emissions, microbial community profile and function from three full-scale WWTPs. *Sci Total Environ* 2019;**651**:2460–72. https://doi.org/10.1016/j.scitotenv.2018.10.132
24. Domingo-Félez C, Smets BF. A consilience model to describe N2O production during biological N removal. *Environ Sci Wat Res* 2016;**2**:923–30. https://doi.org/10.1039/C6EW00179C
25. Mania D, Woliy K, Degefu T *et al.* A common mechanism for efficient N(2) O reduction in diverse isolates of nodule-forming bradyrhizobia. *Environ Microbiol* 2020;**22**:17–31. https://doi.org/10.1111/1462-2920.14731
26. Yoon H, Song MJ, Kim DD *et al.* A serial biofiltration system for effective removal of low-concentration nitrous oxide in oxic gas streams: mathematical modeling of reactor performance and experimental validation. *Environ Sci Technol* 2019;**53**:2063–74. https://doi.org/10.1021/acs.est.8b05924
27. Yoon H, Song MJ, Yoon S. Design and feasibility analysis of a self-sustaining biofiltration system for removal of low concentration N2O emitted from wastewater treatment plants. *Environ Sci Technol* 2017;**51**:10736–45. https://doi.org/10.1021/acs.est.7b02750
28. Conthe M, Wittorf L, Kuenen JG *et al.* Growth yield and selection of nosZ clade II types in a continuous enrichment culture of N2O respiring bacteria. *Environ Microbiol Rep* 2018;**10**:239–44. https://doi.org/10.1111/1758-2229.12630
29. Conthe M, Wittorf L, Kuenen JG *et al.* Life on N2O: deciphering the ecophysiology of N2O respiring bacterial communities in a continuous culture. *ISME J.* 2018;**12**:1142–53. https://doi.org/10.1038/s41396-018-0063-7
30. Qi C, Zhou Y, Suenaga T *et al.* Organic carbon determines nitrous oxide consumption activity of clade I and II nosZ bacteria: genomic and biokinetic insights. *Water Res* 2021;**209**:117910. https://doi.org/10.1016/j.watres.2021.117910
31. Semedo M, Wittorf L, Hallin S *et al.* Differential expression of clade I and II N2O reductase genes in denitrifying Thauera linaloolentis 47LolT under different nitrogen conditions. *FEMS Microbiol Lett* 2020;**367**:1–6. https://doi.org/10.1093/femsle/fnaa205
32. LaSarre B, Morlen R, Neumann GC *et al.* Nitrous oxide reduction by two partial denitrifying bacteria requires denitrification intermediates that cannot be respired. *Appl Environ Microbiol* 2024;**90**:e01741–23. https://doi.org/10.1128/aem.01741-23
33. Deacon R, Perry J, Lumb M *et al.* Selective inactivation of vitamin B12 in rats by nitrous oxide. *Lancet* 1978;**312**:1023–4. https://doi.org/10.1016/S0140-6736(78)92341-3
34. Kuenen JG. Continuous cultures (Chemostats). In: Schmidt T.M. (ed.), *Encyclopedia of Microbiology*, Fourth edn. Oxford: Academic Press, 2019, 743–61.
35. van der Star WR, van de Graaf MJ, Kartal B *et al.* Response of anaerobic ammonium-oxidizing bacteria to hydroxylamine. *Appl Environ Microbiol* 2008;**74**:4417–26. https://doi.org/10.1128/AEM.00042-08
36. Vishniac W, Santer M. Santer MJBr. *The thiobacilli* 1957;**21**:195–213. https://doi.org/10.1128/br.21.3.195-213.1957
37. APHA. *Standard Methods for the Examination of Water and Wastewater*. 21st Edition. Washington, D.C.: American Public Health Association/American Water Works Association/Water Environment Federation, 2005.
38. Roels J. *Energetics and Kinetics in Biotechnology*. Amsterdam, The Netherlands: Elsevier Biomedical Press, 1983.
39. Hellinga C, Romein B. MACROBAL: a program for robust data reconciliation and gross error detection. *IFAC Proceedings Volumes* 1992;**25**:459–60. https://doi.org/10.1016/S1474-6670(17)50415-2
40. Sander R. Compilation of Henry's law constants (version 4.0) for water as solvent. *Atmos Chem Phys* 2015;**15**:4399–981. https://doi.org/10.5194/acp-15-4399-2015
41. Bolger AM, Lohse M, Usadel B. Trimmomatic: a flexible trimmer for Illumina sequence data. *Bioinformatics* 2014;**30**:2114–20. https://doi.org/10.1093/bioinformatics/btu170
42. Nurk S, Meleshko D, Korobeynikov A *et al.* metaSPAdes: a new versatile metagenomic assembler. *Genome Res* 2017;**27**:824–34. https://doi.org/10.1101/gr.213959.116
43. Li H. Aligning sequence reads, clone sequences and assembly contigs with BWA-MEM. 2013. arXiv preprint arXiv:1303.3997.
44. Li H, Handsaker B, Wysoker A *et al.* The sequence alignment/map format and SAMtools. *Bioinformatics* 2009;**25**:2078–9. https://doi.org/10.1093/bioinformatics/btp352
45. Kang DD, Li F, Kirton E *et al.* MetaBAT 2: an adaptive binning algorithm for robust and efficient genome reconstruction from metagenome assemblies. *PeerJ* 2019;**7**:e7359. https://doi.org/10.7717/peerj.7359
46. Parks DH, Imelfort M, Skennerton CT *et al.* CheckM: assessing the quality of microbial genomes recovered from isolates, single cells, and metagenomes. *Genome Res* 2015;**25**:1043–55. https://doi.org/10.1101/gr.186072.114
47. Parks DH, Rinke C, Chuvochina M *et al.* Recovery of nearly 8,000 metagenome-assembled genomes substantially expands the tree of life. *Nat Microbiol* 2017;**2**:1533–42. https://doi.org/10.1038/s41564-017-0012-7
48. Chaumeil PA, Mussig AJ, Hugenholtz P *et al.* GTDB-Tk v2: memory friendly classification with the genome taxonomy database. *Bioinformatics* 2022;**38**:5315–6. https://doi.org/10.1093/bioinformatics/btac672
49. Dong X, Strous M. An integrated pipeline for annotation and visualization of metagenomic Contigs. *Front Genet* 2019;**10**:1–10. https://doi.org/10.3389/fgene.2019.00999
50. Kanehisa M. Enzyme annotation and metabolic reconstruction using KEGG. *Methods Mol Biol* 2017;**1611**:135–45. New York, NY, Springer New York. https://doi.org/10.1007/978-1-4939-7015-5_11
51. Paysan-Lafosse T, Blum M, Chuguransky S *et al.* InterPro in 2022. *Nucleic Acids Res* 2023;**51**:D418–27. https://doi.org/10.1093/nar/gkac993
52. Simon J, Einsle O, Kroneck PM *et al.* The unprecedented nos gene cluster of Wolinella succinogenes encodes a novel respiratory electron transfer pathway to cytochrome c nitrous oxide reductase. *FEBS Lett* 2004;**569**:7–12. https://doi.org/10.1016/j.febslet.2004.05.060
53. Zallot R, Ross R, Chen WH *et al.* Identification of a novel Epoxyqueuosine reductase family by comparative genomics.

*ACS Chem Biol* 2017;**12**:844–51. https://doi.org/10.1021/acschembio.6b01100
54. Apweiler R, Bairoch A, Wu CH *et al.* UniProt: the universal protein knowledgebase. *Nucleic Acids Res* 2004;**32**:115D–9. https://doi.org/10.1093/nar/gkh131
55. Roothans N, Gabriels M, Abeel T *et al.* Aerobic denitrification as an N2O source from microbial communities. *ISME J.* 2024;**18**:1–13. https://doi.org/10.1093/ismejo/wrae116
56. Corbera-Rubio F, Laureni M, Koudijs N *et al.* Meta-omics profiling of full-scale groundwater rapid sand filters explains stratification of iron, ammonium and manganese removals. *Water Res* 2023;**233**:119805. https://doi.org/10.1016/j.watres.2023.119805
57. RStudio Team. *RStudio: Integrated Development Environment for R*. Boston, MA: RStudioPBC, 777, 2021, http://www.rstudio.com/.
58. R Core Team. *R: A Language and Environment for Statistical Computing*. Vienna, Austria: R Foundation for Statistical Computing, 2022. https://www.r-project.org/.
59. Banks RGS, Henderson RJ, Pratt JM. Reactions of gases in solution. Part III. Some reactions of nitrous oxide with transition-metal complexes. *J Chem Soc A* 1968;**0**:2886–9. https://doi.org/10.1039/j19680002886
60. Sullivan MJ, Gates AJ, Appia-Ayme C *et al.* Copper control of bacterial nitrous oxide emission and its impact on vitamin B12-dependent metabolism. *Proc Natl Acad Sci USA* 2013;**110**:19926–31. https://doi.org/10.1073/pnas.1314529110
61. Kleiner M, Thorson E, Sharp CE *et al.* Assessing species biomass contributions in microbial communities via metaproteomics. *Nat Commun* 2017;**8**:1558. https://doi.org/10.1038/s41467-017-01544-x
62. Barco RA, Garrity GM, Scott JJ *et al.* A genus definition for bacteria and archaea based on a standard genome relatedness index. *MBio* 2020;**11**:1–20. https://doi.org/10.1128/mBio.02475-19
63. Thomsen TR, Kong Y, Nielsen PH. Ecophysiology of abundant denitrifying bacteria in activated sludge. *FEMS Microbiol Ecol* 2007;**60**:370–82. https://doi.org/10.1111/j.1574-6941.2007.00309.x
64. Wang Z, Li W, Li H *et al.* Phylogenomics of Rhodocyclales and its distribution in wastewater treatment systems. *Sci Rep* 2020;**10**:3883. https://doi.org/10.1038/s41598-020-60723-x
65. Wu L, Ning D, Zhang B *et al.* Global diversity and biogeography of bacterial communities in wastewater treatment plants. *Nat Microbiol* 2019;**4**:1183–95. https://doi.org/10.1038/s41564-019-0426-5
66. Conthe M, Parchen C, Stouten G *et al.* O2 versus N2O respiration in a continuous microbial enrichment. *Appl Microbiol Biotechnol* 2018;**102**:8943–50. https://doi.org/10.1007/s00253-018-9247-3
67. Kim DD, Han H, Yun T *et al.* Identification of nosZ-expressing microorganisms consuming trace N2O in microaerobic chemostat consortia dominated by an uncultured Burkholderiales. *ISME J* 2022;**16**:2087–98. https://doi.org/10.1038/s41396-022-01260-5
68. Jonassen KR. *Biogas Digestate as Substrate and Vector for the Introduction of N2O-Respiring Bacteria to Agricultural Soil*. Norwegian University of Life Sciences, Series: Phd Thesis; 2021, 53.
69. Valk LC, Peces M, Singleton CM *et al.* Exploring the microbial influence on seasonal nitrous oxide concentration in a full-scale wastewater treatment plant using metagenome assembled genomes. *Water Res* 2022;**219**:118563. https://doi.org/10.1016/j.watres.2022.118563
70. van den Berg EM, van Dongen U, Abbas B *et al.* Enrichment of DNRA bacteria in a continuous culture. *ISME J* 2015;**9**:2153–61. https://doi.org/10.1038/ismej.2015.26
71. Roth JR, Lawrence JG, Bobik TA. Cobalamin (coenzyme B12): synthesis and biological significance. *Ann Rev Microbiol* 1996;**50**:137–81. https://doi.org/10.1146/annurev.micro.50.1.137
72. Lu X, Heal KR, Ingalls AE *et al.* Metagenomic and chemical characterization of soil cobalamin production. *ISME J* 2020;**14**:53–66. https://doi.org/10.1038/s41396-019-0502-0
73. Shelton AN, Seth EC, Mok KC *et al.* Uneven distribution of cobamide biosynthesis and dependence in bacteria predicted by comparative genomics. *ISME J* 2019;**13**:789–804. https://doi.org/10.1038/s41396-018-0304-9
74. Lu J, Tappel RC, Nomura CT. Mini-review: biosynthesis of poly(hydroxyalkanoates). *Polym Rev* 2009;**49**:226–48. https://doi.org/10.1080/15583720903048243
75. Morris JJ, Lenski RE, Zinser ER. The black queen hypothesis: evolution of dependencies through adaptive gene loss. *MBio* 2012;**3**:1–7. https://doi.org/10.1128/mBio.00036-12
76. Bjorkeroth J, Campbell K, Malina C *et al.* Proteome reallocation from amino acid biosynthesis to ribosomes enables yeast to grow faster in rich media. *Proc Natl Acad Sci USA* 2020;**117**:21804–12. https://doi.org/10.1073/pnas.1921890117
77. O'Brien EJ, Utrilla J, Palsson BO. Quantification and classification of E. Coli proteome utilization and unused protein costs across environments. *PLoS Comput Biol* 2016;**12**:e1004998. https://doi.org/10.1371/journal.pcbi.1004998
78. Peebo K, Valgepea K, Maser A *et al.* Proteome reallocation in Escherichia coli with increasing specific growth rate. *Mol BioSyst* 2015;**11**:1184–93. https://doi.org/10.1039/C4MB00721B
79. Men Y, Yu K, Baelum J *et al.* Metagenomic and Metatranscriptomic analyses reveal the structure and dynamics of a Dechlorinating community containing Dehalococcoides mccartyi and Corrinoid-providing microorganisms under cobalamin-limited conditions. *Appl Environ Microbiol* 2017;**83**:1–14. https://doi.org/10.1128/AEM.03508-16




*ISME Communications*, 2025, **5(1)**, ycaf022
https://doi.org/10.1093/ismeco/ycaf022
Original Article